Numerical prediction of trailing edge noise of an asymmetric high lift airfoil for different angles of attack with a LES scheme.

Keywords: LES, trailing edge noise, low Mach number, acoustic analogy.

Abstract

In this paper, the aerodynamic field around a FX 63-137 airfoil for four angles of attack and low Reynolds numbers was simulated with a Large Eddy Simulation (LES). Following, an acoustic analogy method was employed to calculate the airfoil trailing edge (TE) noise. In this second scheme step, the far-field acoustic pressure was predicted from the LES source terms using two different methods based on Lighthill's analogy: Curle's surface approach and Ffowcs-Williams and Hall's volumetric analogy (FW-Hall). Numerical results have been validated with hot-wire anemometry for the aerodynamic fields, thus verifying the accuracy of the CFD simulation for the prediction of noise propagation to the far field. Additionally, aeroacoustic results were validated with experimental measurements carried out in an anechoic wind tunnel using a frequency analyzer. The FW-Hall formulation shows a better agreement with the experiments, especially in the range of frequencies corresponding to the trailing edge, whereas Curle's analogy overpredicts airfoil sound. An exhaustive analysis of the aerodynamic flow field has been performed in order to better understand the generation mechanisms of the TE noise. The aeroacoustic calculations presented in this work contribute to develop a more reliable and efficient prediction methodology based on the Computational Aeroacoustics Approach (CAA).

Nomenclature

Abbreviations

LES	Large Eddy Simulation
CFD	Computational Fluid Dynamics
RANS	Reynolds-Averaged Navier-Stokes
CAA	Computational Aeroacoustic Approach
CDS	Central Difference Scheme
FW-Hall	Ffowcs Williams and Hall
PSD	Power Spectrum Density
TS	Tollmien-Schlichting
TE	Trailing Edge
SPL	Sound Pressure Level

Roman letters

c	Airfoil chord, [m]
c_0	Sound speed, [m/s]
f	Frequency, [Hz]
$k = \dfrac{\omega}{c_0}$	Acoustic wavenumber, [m^{-1}]
$L1$	Wake position. [-]
$L2$	Airfoil position, [-]
L_{exp}	Simulated airfoil span, [m]
L_z	Airfoil span, [m]
M	Mach number [-]
n	Outward normal vector from the fluid, [-]
N	Number of samples, [-]
p	Pressure, [Pa]
p'	Pressure fluctuations, [Pa]
p^*	Far-field acoustic pressure [Pa]

Q	Q-criterio, [s^{-2}]
R	Distance between source and observer [m]
Re	Reynolds number, [-]
r, θ, z	Polar coordinates of observer field point, [m], [rad], [m]
r_0, θ_0, z_0	Polar coordinates of source field points, [m], [rad], [m]
S_{ij}	Rate-of-strain tensor, [s^{-1}]
T	Extraction period [s]
t	Time [s]
U_x	Instantaneous streamwise velocity component, [m/s]
U_{max}	Maximum velocity, [m/s]
v_i, v_j	Velocity components, [m/s]
v_r, v_θ	Polar velocity components, [m/s]
V	Integration volume around the airfoil, [m^3]
x, y, z	Streamwise, normal and spanwise cartesian coordinates, airfoil surface [m]
x_i, x_j	Streamwise, normal and spanwise cartesian coordinates, observer location, [m]
$\vec{x}, \vec{y}$	Observer and source vector coordinates, [m]

Symbols

$\Delta x^+, \Delta y^+, \Delta z^+$	Dimensionless distance from airfoil, [-]
δ_{99}	Boundary layer thickness, [m]
τ	Time Lag [s]
ρ	Density, [kg/m^3]
Ω_{ij}	Rate-of-rotation tensor, [s^{-1}]
γ^2	Coherence function
ϕ_{pp}	Wall-pressure power spectral density, [Pa^2/Hz]

1. Introduction

Wind energy has become one of the most rapidly growing forms of renewable energy production in the last century. However, one of the major problems for public acceptance of wind energy is the noise emitted by wind turbines. The growth of population density leads to expansion of urban areas, and a balance between wind technology and people is necessary. Therefore, new wind turbine designs must be more efficient at places with low wind speed. Additionally, the noise radiated by new designs must be reduced. The most important factors related to noise generation and propagation are the turbine size and the distance to the observer. Although wind turbines for inhabited places have been progressively reducing their size, they are placed very close to residential areas. Consequently, there has been an increase in the sensitivity of communities, as well as in the certification requirements for the installation of these turbines.

Frequently, small wind turbines operate at low to moderate Reynolds numbers. Arcondoulis et al. [1] realized a classification of the noise generated by airfoils at this range of Reynolds numbers, considering the trailing edge (TE) noise the major noise generation mechanism for rotor blades of wind turbines [2, 3] thus, limiting their use in urban areas. TE noise is due to the scattering of boundary layer vortical disturbances into acoustic waves at the airfoil TE. It is an unavoidable noise source and easily dominates the broadband noise in a frequency range from 750 Hz up to 2500 Hz at low Mach numbers [4]. Therefore, the understanding of the flow around the airfoil is strongly necessary for aerodynamic and acoustic design purposes.

Nowadays, one of the most commonly used methods for sound prediction is based on the Computational Aeroacoustics Approach (CAA). Computational Aeroacoustics is a tool that uses numerical computations to obtain acoustic data from the aerodynamic flow field. In particular,

hybrid methods have revealed as the most promising and useful technique [5]. A complete direct CAA process is too difficult, due to the disparity of scales between flow- and acoustics-related phenomena, so the use of a hybrid procedure is necessary in most of the cases. This approach divides the problem in two parts, an aerodynamic part, computed by CFD, and an aeroacoustic part, calculated from acoustic models. As the aeroacoustics problems are, by definition, highly time dependent, it is necessary to use sophisticated methods to predict both generation and propagation of broadband noise in a reliable way. Sound generated aerodynamically can be calculated by means of aeroacoustic analogies, all based on the Lighthill's work [6]. Generally, the most used methodology for the prediction of far field noise is to compute the near unsteady flow field using a LES technique in conjunction with an acoustic model. Kim et al. [7] used this method to explore the flow behavior near the airfoil TE to predict the radiated noise. Several acoustic models based on Lighthill's work, can be used in the acoustic analogy to obtain the sound in the far field. Depending on the model chosen, the source terms can be extracted either from a volume integral or a surface integral (**Figure 1**). Curle [8] proposed an integral formulation to calculate the sound from turbulent flow developed over a solid surface being available only for acoustically compact source regions. Amiet [9] developed a theory for sound radiation from the TE of a simplified airfoil that also considers non-compactness effects. Both methods require a pressure distribution on the airfoil surface as an input. Alternatively, Ffowcs Williams and Hall [10] simplifies the airfoil to a semi-infinite flat plate, resolving the Lighthill equation through an approximate hard-wall Green's function with velocity-based volume source terms, while Howe [11] derived a wave equation that utilizes the vorticity as a source term over a volume integral.

Several authors compared the different models to conclude which is the best option to predict far field sound via acoustic analogy. Wang [12] simulated, through LES schemes, a flat strut with a circular leading edge and an asymmetrically beveled TE of 25 degrees, using the volume integral approach of FW-Hall approach to predict the noise. Conversely, Christophe et al. [13] used a LES approach combined with the surface integral models of Amiet and Curle. Surface integral models are based on obtaining the variables over the airfoil surface, so they can be sensitive to any variation in this zone. Winkler et al. [14] studied the effect of grid refinement in LES simulations on the prediction of TE noise in an airfoil using different model approaches. As part of their conclusions, they stated that the solution of Lighthill's analogy with a finite element method has shown that significant noise sources are present on the airfoil which can partly be due to the boundary layer transitions. Other authors, as Kim et al. [15], used the Ffowcs Williams and Hawking's equation to predict the acoustic noise related to flat back airfoils in large wind turbines through a hybrid RANS-LES method. Although most of the authors recognize that the FW-Hall approach is the most suitable to predict TE noise [14, 16], there is no consensus on the use of a particular model in this field. For this reason, more accurate and deeper investigations are completely significant to understand the flow behavior over the airfoils and the mechanisms of the noise generated by them.

Different ways to reduce TE noise have been investigated in the last years. The most extended method is the use of trailing edge noise serrations, which affect the noise scattering at the TE [17]. Following the same concept, the application of flexible TE brushes has shown significant noise reduction in wind tunnel tests [18]. On the other hand, it has been demostrated that modifications on the airfoil shape can reduced TE noise, by changing the structure of the boundary layer turbulence [19]. In this line, the acoustic prediction model presented in this paper provides a useful and cost-effective tool for the design stage of wind turbines, being able to compare efficently different airfoil geometries.

Consequently, the purpose of this work is to develop a more reliable and efficient methodology based on the CAA. Firstly, the aerodynamic field around a FX 63-137 airfoil for four angles of

attack and low Reynolds numbers was simulated with a LES scheme. Then, an acoustic analogy method was employed to calculate the TE noise, using two different models based on Lighthill's analogy: Curle's surface approach and FW-Hall's volumetric analogy. Both numerical and aeroacoustic results have been validated with thermal anemometry and frequency analyzer experiments respectively. The final aim of this paper is to become a contribution to the ongoing research involving aerodynamic and aeroacoustic airfoil design in the wind renewable energy industry.
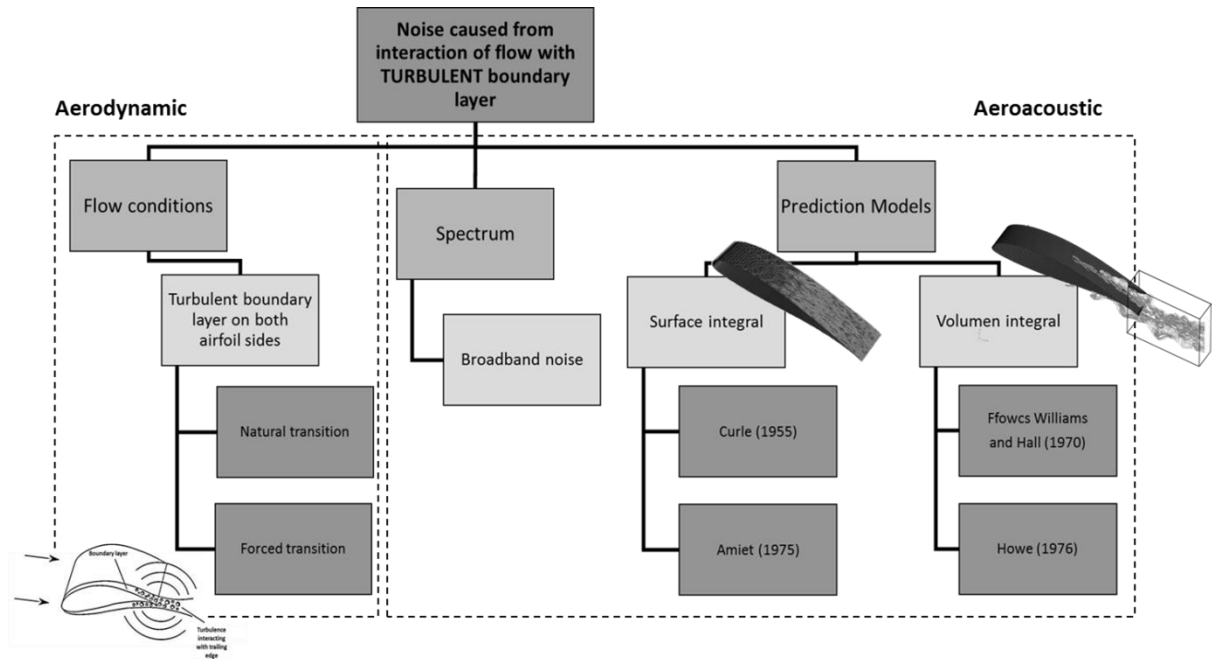
Figure 1. Trailing edge noise characteristics and acoustic models.

2. Experimental methodology

2.1. Experimental setup

A 1:1 scale FX 63-137 airfoil model with a span of 1.1 m and a chord length of 0.305 m was built to carry out hot-wire measurements of the flow field. This airfoil was designed by F.X. Wortmann in 1972 for the Liver Puffin human-powered aircraft [20]. It has since been used for many low Reynolds number applications, especially for small wind turbines, due to its overall good performance and its high-lift and soft-stall characteristics. An aeroacoustic wind tunnel, which has been characterized by Lastra et al. [21], has been employed to realize the measurements over the airfoil.

The wind tunnel consists of a closed loop circuit, arranged in a vertical layout (**Figure 2**). The total length of the tunnel is 24.6 m, with 8.3 m high and maximum operative velocities in the range of 22 m/s for the test section, i.e., a maximum Reynolds number of 1.7×10^6 based on the outlet hydraulic diameter of the nozzle (i.e., the outlet width).

Turbulence intensity levels are lower than 0.7% for the whole range of operational velocities in the wind tunnel [21]. The FX 63-137 airfoil model is placed at the outlet of the nozzle center, inside the test chamber (**Figure 2**).
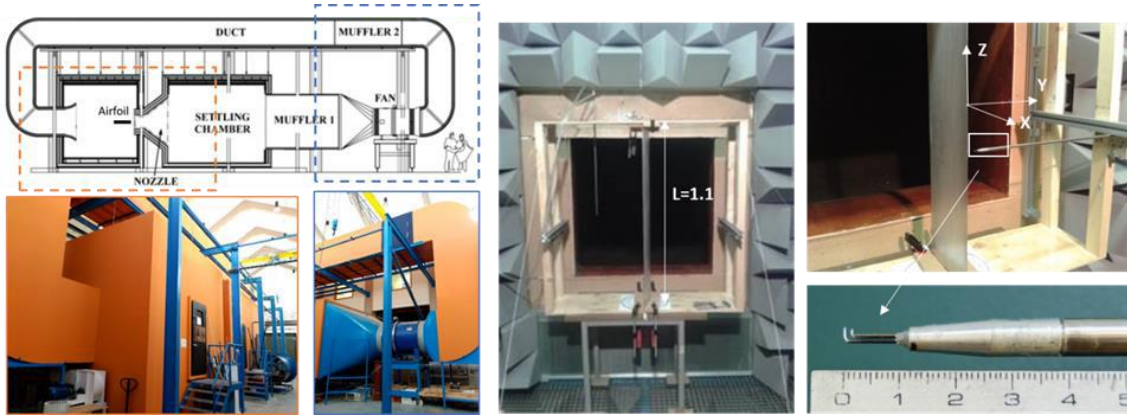
Figure 2. Aeroacoustic wind tunnel and experimental setup. Right-down corner: detail of the X-probe for hot-wire measurements.

2.2. Dual hot-wire anemometry

Hot wire anemometry is a well-established, accurate and reliable technique to measure the flow velocity [22]. The velocity distributions were measured with a home-made X-wire probe, connected to a constant temperature anemometer. **Figure 3** illustrates the procedure employed to collect the data and an example of the signal captured after transforming the data with the appropriate calibration. The analog voltage signal was first low-passed at 5 kHz using an analog filter to avoid aliasing. The uncertainty of the absolute velocity has been estimated to be 0.75% in the center of the angular calibration range, while the angular uncertainty has been estimated to be 1° at the center of the measurement range. More details about the procedure and the uncertainty analysis of the probe are described in references [23] and [24]. The measurements were performed at 10 kHz over 25 seconds for every position. A convergence study of the mean velocity was made, verifying that the number of samples was enough (**Figure 3**, right).
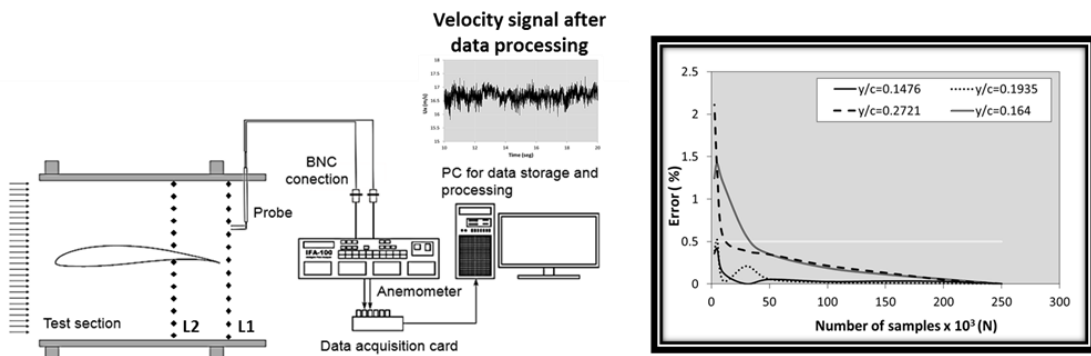

Figure 3. Measurement procedure and convergence study of mean velocities at four positions along the measurement rake.

Measurements were made by sweeping two rakes at different streamwise locations: $L1$, in the airfoil wake ($x = 1.108c$) and $L2$, at around 75% of the airfoil chord ($x = 0.764c$). This last location was chosen because it is a representative position of the high airfoil curvature. Both positions may be seen in **Figure 3**. In the following, Wake ($L1$) and Airfoil ($L2$) will be used to refer to these positions. The airfoil was placed at four different incidence angles: -2.5, 2.5, 7.5, and 12.5 degrees, none close to stall, and at a 3.5×10^5 Reynolds number.

2.3. Acoustic measurements

To carry out the acoustic measurements two capacitive ½" microphones coupled with a protection windscreen were used. The preamplifier exit of the microphone was connected to a PC, which works as a multichannel frequency analyzer. The measurements were made for the flow conditions mentioned above.

The microphones, as depicted in **Figure 4**, were located on both lateral sides with respect to the TE. The microphones were positioned at the same radial distance from the TE, perpendicularly to the flow direction and outside of the stream ($R = 1.5$ m and $\theta = 74°$). Each of the microphones was calibrated before starting the acoustic tests. To provide isolation from wind noise, a windscreen was placed on the microphones prior to data acquisition. The microphone data were collected at a sampling frequency of 5.12 kHz for a sampling time of 20 s. The time signal was recorded simultaneously by the two microphones (**Figure 4**, right). Two measurement sets were made for each angle of incidence, with and without the airfoil, in order to estimate the background noise. With the finality to isolate the TE noise, a cross-spectral analysis of Sound Pressure Level (SPL) measurements was employed using the microphone pair [25]. Additionally, as TE noise must be significantly higher than background noise in order to be considered, a criterion for rejection was established. The cross spectrum of the measurements from both microphones with and without the airfoil were compared., and frequency bins with a SPL increase less than 3 dB was removed from consideration. For the considered frequency bins, the magnitude of background noise was subtracted from the noise measured with the airfoil. Hence, the correlated wind tunnel noise was eliminated from the samples and only the effects due to the airfoil presence remained.
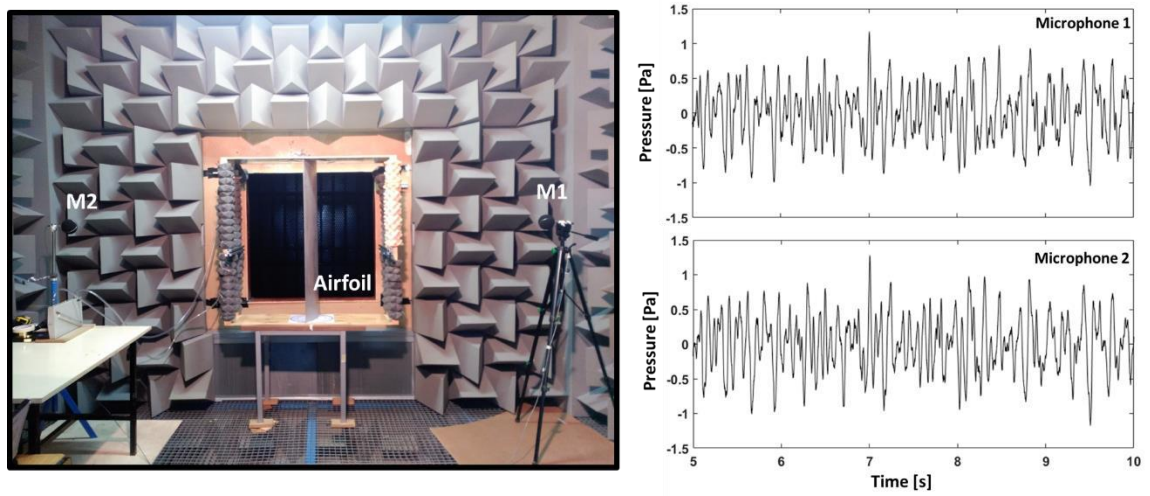

Figure 4. Acoustic setup in the wind tunnel test anechoic chamber (left). 5s zoom of the measured signal from both microphones used to perform the cross-correlation (right).

3. Numerical methodology

In order to obtain the flow field necessary for the acoustic models, 3D-LES CFD simulations were performed using Fluent to solve the Navier-Stokes equations. As shown by Moreau et al. [26], when the wind tunnel jet width is not large enough compared to the streamwise projected area of the airfoil (width-to-chord ratio of about 1), the flow around an airfoil can differ from the flow around the same airfoil in free stream conditions. In the current case, as the ratio between the wind tunnel jet width and the model chord is 3.3, the sidewall effects from the tunnel may be neglected.

3.1. Grid topology

A block-structured C-mesh of 1.9×10^7 elements, refined at the boundary layer and TE regions, was used for the numerical simulations (
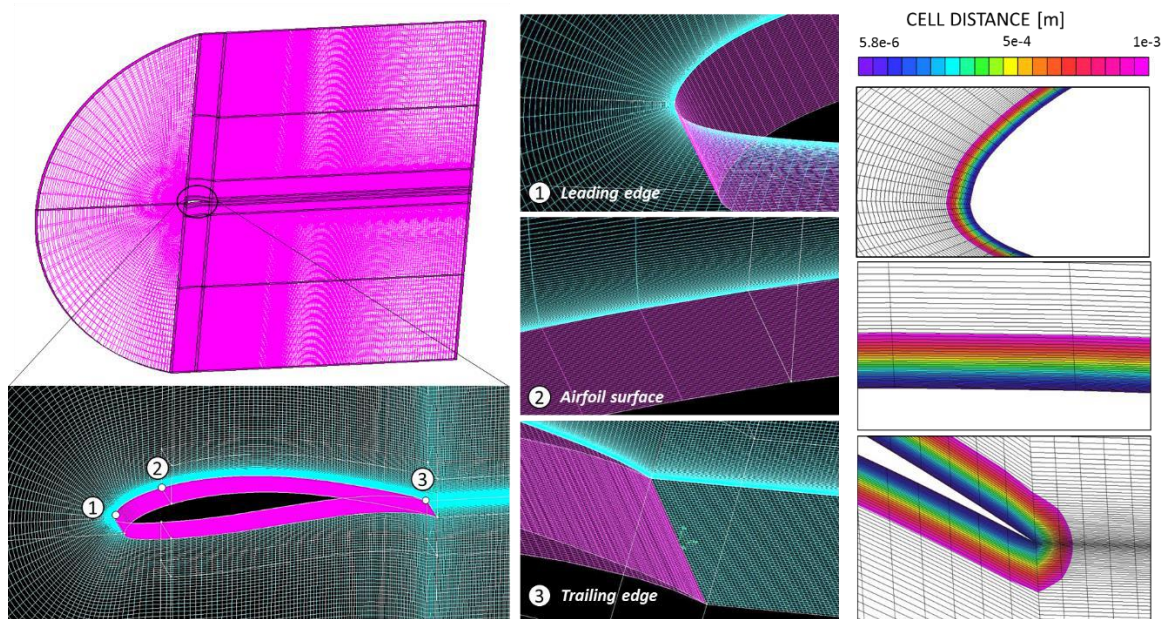

Figure 5). To ensure a good mesh resolution, the criteria recommended by Wagner et al. [27] were followed: the cell size in the stream, normal and span direction near the wall contours were $\Delta x^+ = 45$, $\Delta y^+ = 0.8$, $\Delta z^+ = 30$ respectively.

The domain boundaries were placed at: 4.92c upstream from the leading edge, 8.84c downstream from the TE and 6.25c in the normal direction from both airfoil faces. The spanwise dimension of the domain was set as $L_z = 0.164c$. The largest scales in a boundary layer are in the order of δ_{99} (boundary layer thickness). As these scales are likely to appear spanwise, the ratio δ_{99} / L_z should be at least less than one [28]. In this work case, the boundary layer thickness δ_{99} obtained from the experiments is about 2% of the chord, eight times shorter than L_z.
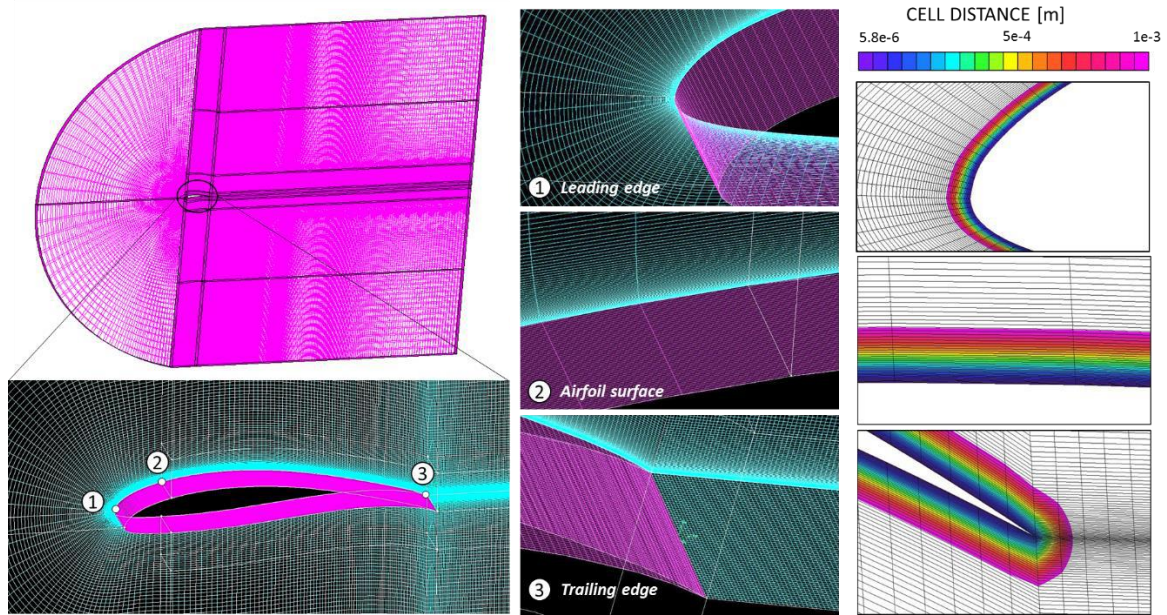
Figure 5. Grid topology used in the simulations. Zoom of different regions where refine mesh.

3.2. Numerical setup and boundary conditions

The LES scheme was used with the Smagorinsky-Lilly subgrid model. The central difference scheme (CDS), due to its non-dissipative and energy conserving properties, was employed for the LES computations along with a bounded second-order upwind discretization scheme. Pressure-based solver with the SIMPLE velocity coupling was defined together with a Green-Gauss cell based discretization scheme.

Regarding the boundary conditions, a pressure outlet condition was applied in the far boundary, while the velocity-inlet condition was specified for the rest of the far-field boundaries. A low Mach number of 0.049 was used and the flow conditions were characterized by a 0.7 % turbulence intensity and an integral length scale of 0.075 m, obtained in [21] by hot wire measurements. The no-slip condition was used for the top and bottom airfoil faces and the symmetry condition was applied in the spanwise boundaries.

Convergence was guaranteed by monitoring the relative numerical error of the solution, which dropped below 10^{-4}. In the case of LES computations, the selection of an accurate temporal resolution is also critical to be able to resolve the turn-out time of the eddies. Given the freestream velocity, the size of the cell in x direction and satisfying the Courant number, the time step used in this simulations corresponds with $4.05 \, x \, 10^{-5}$ s. The simulations were run for approximately 44 flow-through times, based on the freestream velocity and the airfoil chord length, until reaching a statistically steady state. Seven computers with 4-core i5 processors at 2.67 GHz and 4 Gb DDR3 RAM memory were used for the simulations, which took approximately one month to completion and source term collection.

4. Acoustic models

Far-field TE noise computations were performed by two different models based on Lightill's acoustic analogy. On the one hand, Curle model that is based on a surface integral over the airfoil surface pressure field, and on the other hand the FW-Hall model that requires a volume integral over the velocity field around the TE. In the next, a description of the models is presented.

4.1. Surface Integral model

Curle [8] proposes an extension for the Lighthill's analogy. The difference between them is the influence of the presence of solid limits in the Curle's analogy. It uses a free-space Green's function to give a solution. In the presence of a rigid airfoil at low Mach number, the far-field acoustic pressure only involves a surface integral of the wall-pressure fluctuations:

$$p'(x,t) \cong \frac{x_i x_j}{4\pi c_0^2 |\vec{x}|^2} \frac{\partial^2}{\partial t^2} \int_V \left[\frac{T_{ij}}{r}\right] d\vec{y} - \frac{1}{4\pi} \frac{\partial}{\partial t} \int_S \left[\frac{\rho v_i}{r}\right] n_i \, dS$$
$$- \frac{x_j}{4\pi c_0 |\vec{x}|} \frac{\partial}{\partial t} \int_S \left[(p_{ij} + \rho v_i v_j)\frac{n_i}{r}\right] dS$$

(1)

where the brackets indicate the evaluation of the variables in the retarded time $t - r/c_0$. The parameter r is given by $r = |x - y|$, where x and y are the positions of the observer and the source respectively. In (1), ρ denotes the density, p_{ij} the compressive stress tensor, c_0 the sound velocity, v_i the velocity component in x_i direction and T_{ij} the Lighthill's stress tensor. The distance between the source on the airfoil (y) and the observation point (x) is represented by $|\vec{x}|$. Note that n_i is the outward normal from the fluid.

If the airfoil it is assumed to be compact and the observer to be in the far-field, retarded time variations can be neglected. Additionally, the velocities in the surfaces are zero, so the volume integral, which represents the quadrupolar source term, can be neglected to calculate the acoustic pressure radiated to the far-field in the case of low-Mach flows. This is because of the sound production of this term is smaller in comparison with the dipolar source contributions that represent the resultant force exerted over the flow by the solid boundaries. Thus, the Curle's analogy to predict the far-field acoustic pressure for a particular observer reads as:

$$p'(x,t) \cong -\frac{x_j}{4\pi c_0 |\vec{x}|^2} \frac{\partial}{\partial t} \int_S p n_i \, dS$$

(2)

One of the drawbacks of using Curle's analogy is that this result is difficult to interpret for non-compact surfaces, because it is not possible to estimate quantitatively the dipole term for surfaces which are not small compared with an acoustic wavelength. Therefore, for low Mach number flows, Curle's approach is strictly valid for acoustically compact bodies, i.e., for acoustic wavelengths much larger than the airfoil chord.

4.2. Volume integral model

One of the first theoretical investigations related to the TE noise was made by Ffowcs Williams and Hall [10]. As in the Curle's analogy, the starting point of their work is based on the Lighthill's one. The formulation by FW-Hall simplifies the airfoil to a semi-infinite flat plate with zero thickness. Lighthill's equation is then solved using the exact Green's function for a scattering half-plane. For sources close to the TE, a series expansion is used to approximate the Green's function. The far-field acoustic pressure at an observer location $x(r,\theta,z)$ and for an angular frequency ω, is given by:

$$4\pi p^*(r,\theta,z;\omega) = k^2 \frac{2e^{-i\pi/4}}{\sqrt{\pi}} (\sin\phi)^{1/2} \sin\frac{\theta}{2} \frac{e^{ikR}}{R}$$
$$\times \left[(\rho v_r^2 - \rho v_\theta^2)^* \int \sin\frac{\theta_0}{2} (2kr_0)^{-\frac{3}{2}} dV_0\right.$$
$$\left. + (2\rho v_r v_\theta)^* \int \cos\frac{\theta_0}{2} (2kr_0)^{-\frac{3}{2}} dV_0\right]$$

(3)

where V is the integration volumen around the TE, ω is the angular frequency and $k = \omega/c_0$ is the acoustic wave number. The polar velocity components around the TE are v_r and v_θ. The caret denotes temporal Fourier transform, and x (r, θ, z) and y (r_0, θ_0, z_0) are the vector positions of the far-field observer and the source respectively. The distance between the two points is defined as $R = |x - y|$ and $\sin \phi = r/[r^2 + (z - z_0)^2]^{\frac{1}{2}}$.

To reduce the calculations, if the spanwise source extent is acoustically compact when projected in the direction of propagation, which is the case for the source-region contained within the computational domain, a simplification of Equation 3 can be made, proposed by Wang and Moin [29]. This is generally not the case for the full span airfoil of the experiments, but it is a reasonable assumption for the source region contained in the computational domain. Then, Equation 3 can be approximated by:

$$p^*(\vec{x}, \omega) \approx \frac{e^{i(k|\vec{x}| - \pi/4)}}{2^{\frac{5}{2}} \pi^{\frac{3}{2}} |\vec{x}|} (k \sin \phi)^{\frac{1}{2}} \sin \frac{\theta}{2} \hat{S}(\omega) \tag{4}$$

with

$$S(t) = \int_V \frac{\rho}{r_0^{\frac{3}{2}}} \left[\left(v_\theta^2 - v_r^2 \right) \sin \frac{\theta_0}{2} - 2 v_r v_\theta \cos \frac{\theta_0}{2} \right] d^3 \vec{y} \tag{5}$$

5. Aerodynamic results

The first step in the prediction of aerodynamic sound is the identification of acoustic sources in the flow which generate the sound. The simulations performed helped to characterize the flow around the airfoil and identify the necessary inputs for sound modelling.

Firstly, a validation was performed by comparing the results of the simulations with the experimental measurements. The longitudinal velocity components at $L1$ and $L2$ obtained with both methods are shown in **Figure 6**. The values have been made dimensionless in order to make easier the comparison between the different angles. To achieve a better visualization of the wake, the data were aligned to place the minimum local velocity at $y/c = 0$ (**Figure 6**). The typical behavior of flow around an airfoil may be identified for every angle at L1 and L2 positions: the velocity profiles show a reduction near the wall (boundary layer) and inside the wake instability area. In the wake region (L1), it may be appreciated how the wake dimensions increase as the angle of attack becomes higher.

The boundary layers developed at the $L2$ position are very thin, so the velocity inside the them decreases drastically. This effect has been captured in the experimental measurements on the pressure side for all the angles; however, on the suction side it is only visible for the 12.5 angle. The flow follows the airfoil shape at the suction side due to its smooth curvature, and the interference effects of the probe make difficult to capture the boundary layer. On the pressure side, the high curvature of the airfoil at the probe location widens the boundary layer, which makes possible to obtain measurements inside it without breaking the probe.

As shown in **Figure 6**, there is a reasonable agreement between results obtained by the present flow solver and experimental results. The correct validation of the numerical results is of great importance, as they will be used as the input for the aeroacoustic prediction models. Specially, the volume and surface noise source terms, which are directly obtained from the aerodynamic flow field, must be correctly identified [30].
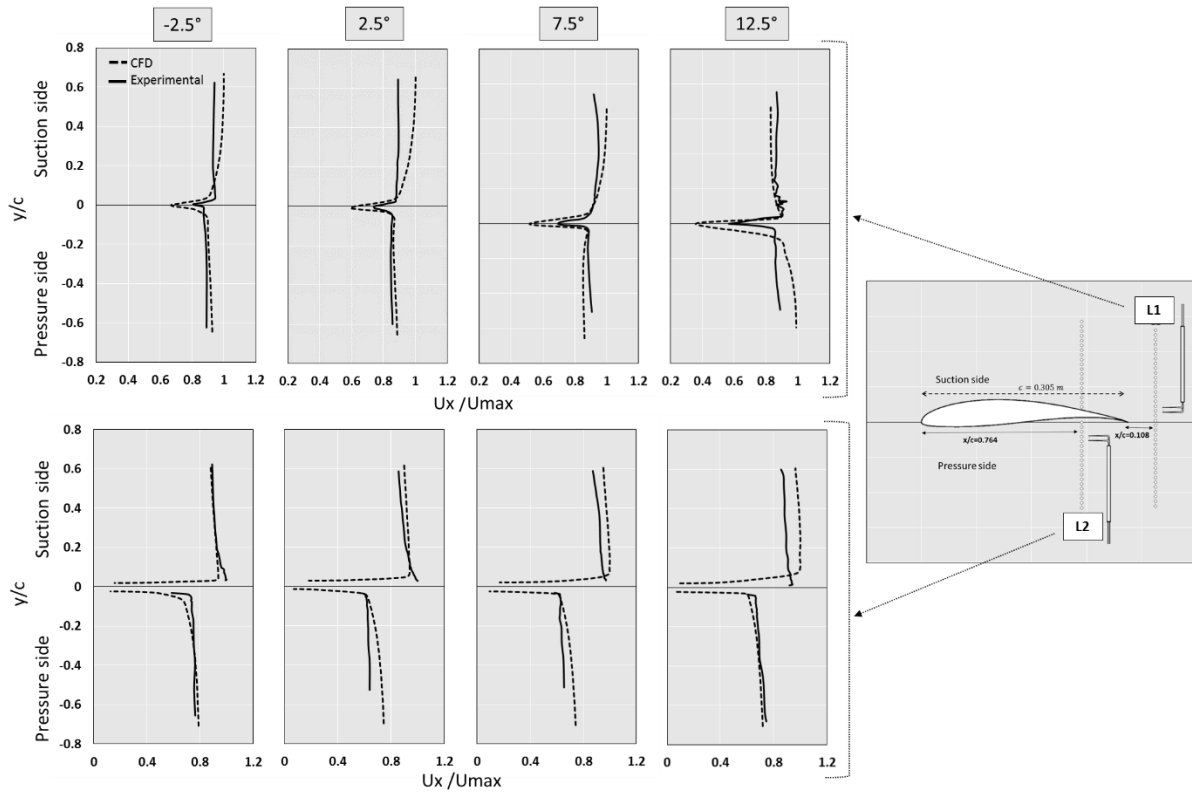
Figure 6. Experimental and numerical longitudinal velocity components for positions L1 and L2.

Once the numerical simulations have been validated and the simulations have reached stability, the aerodynamic results obtained may be discussed. **Figure 7** represents the instantaneous longitudinal velocity component (X-velocity) at a particular instant on both suction (up) and pressure (down) sides for the whole range of angles of attack. The graph shows, qualitatively, the behavior of the flow on the airfoil surface. The uniform color region indicates the laminar boundary layer (absence of instabilities). As the flow moves closer to the TE, instabilities arise. The lowest velocity values appear near the TE. The zone with adverse gradients (purple zone) is really small, and thus no separated flow appears, except for the 12.5 angle. A white dotted line has been added to the figure, showing the point at which flow instabilities start. On the suction side, this line advances towards the leading edge as the angle of attack increases. The opposite behavior is present on the pressure side, where the point at which instabilities start is delayed as the angle increases.
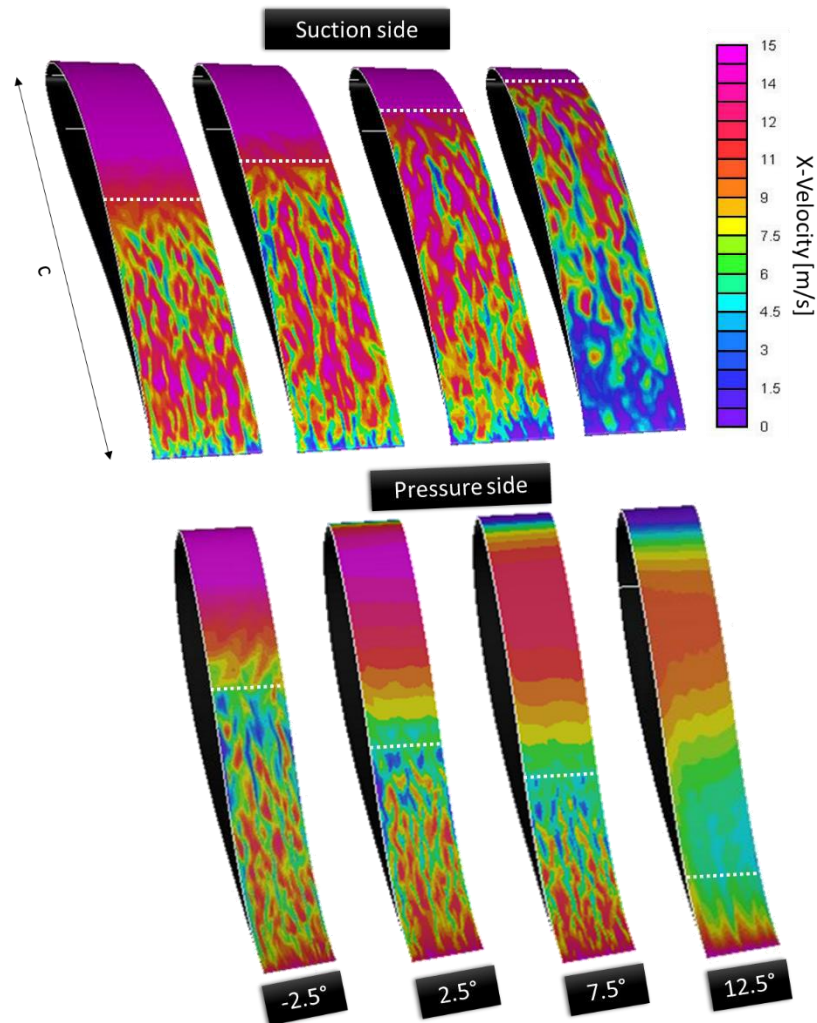
Figure 7. Instantaneous longitudinal velocity component (X-velocity) on the airfoil surface.

The flow behavior may be extracted from the numerical simulations as well. To get a global insight into the flow inside the boundary layer, the Q-criterion may be employed to visualize coherent structures. The Q-criterion is defined as $Q = \frac{1}{2}\left(\Omega_{ij}\Omega_{ij} - S_{ij}S_{ij}\right)$, being Ω_{ij} the mean rate of rotation tensor and S_{ij} the mean strain rate. The Q-criterion is typically used in LES simulations to present the level of vorticity and the size of turbulent structures in the flow [31]. The flow patterns are illustrated in **Figure 8** by the iso-surface of constant Q-criterion, with $Q = 50000\ s^{-2}$, and colored by instantaneous X-velocity values at a given instant.

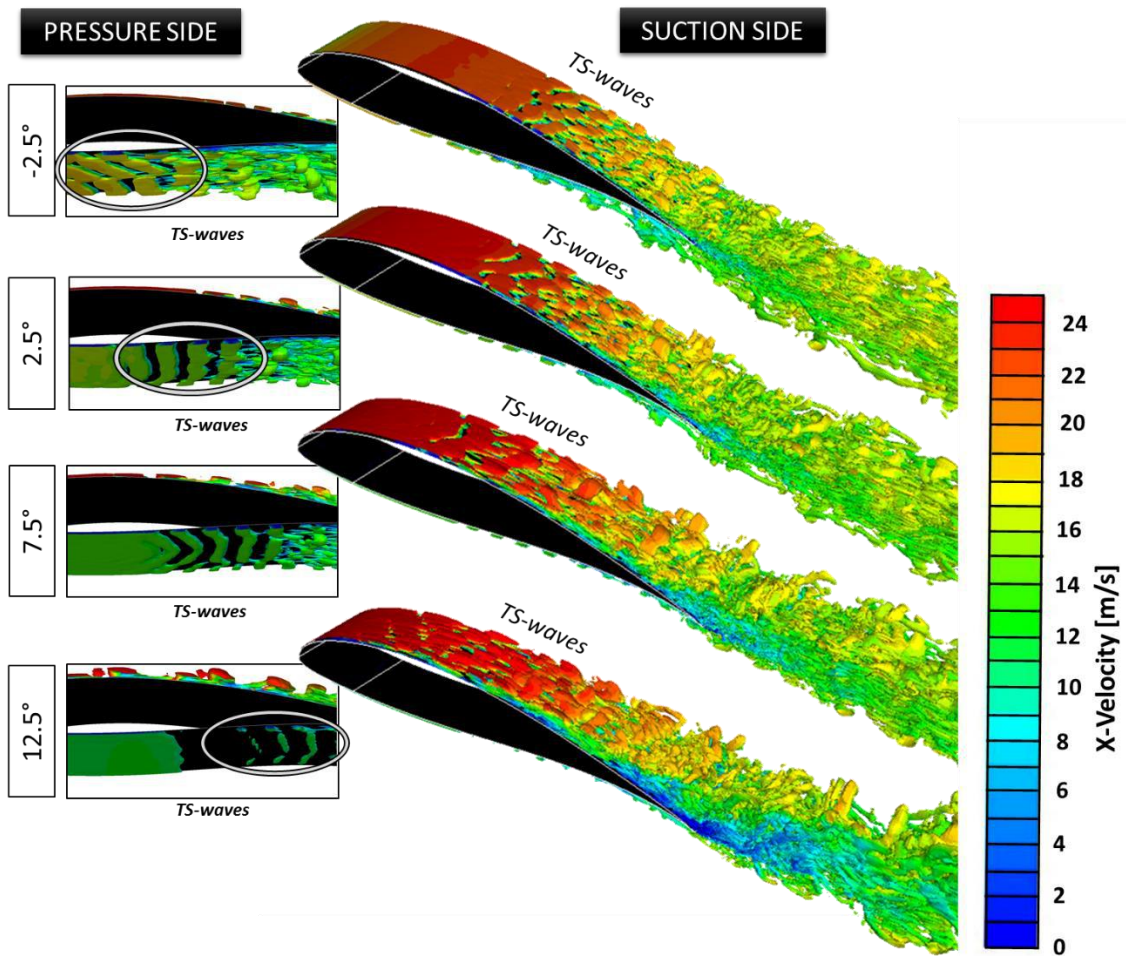**Figure 8.** Visualization of the flow field around the airfoil by iso-surfaces of $Q = 5x10^5 \; s^{-2}$, colored by instantaneous X-velocity values.

The flow around the airfoil is characterized by the development of a turbulent and transient boundary layer on the suction and pressure surfaces. With an increase in the angle of attack, the size of the Q-criterion iso-surface decreases on the pressure side, while it increases on the suction side. On the pressure side, the flow is attached to the airfoil surface; however, the high curvature region of the airfoil causes a widening in the boundary layer. On the contrary, on the suction side, a smoother curvature is present in the airfoil geometry, so the flow is highly adhered to the surface, originating a thin boundary layer which increases with the incidence angle. For the negative angle, the pressure and suction sides interchange. In **Figure 8**, the growth of the wake dimensions with the angle of attack may be also appreciated.

High positive values of Q identify regions of high vorticity and low shear-strain rates, whereas regions of high negative Q indicate low vorticity and high shear-strain rates. Therefore, rotational motions can be distinguished from non-rotational ones. The Q-criterion can be used to compare the unsteady structures around the airfoil and the organized vortex structures on the pressure and suction sides. In **Figure 8**, an important and characteristic phenomenon for aeroacoustic predictions may be observed. The boundary layer in both pressure and suction sides develops 2D Tollmien-Schlichting (TS) instability waves. These waves arise as two-dimensional vortical structures roll up, after an initial stable state [31]. Further secondary 3D instabilities are superimposed to the waves and may lead to a turbulent boundary layer close to the TE. It is assumed that the diffraction of Tollmien-Schlichting instabilities at the TE generates

acoustic waves, which propagate in the far field and trigger an aeroacoustic feedback loop. This is an important effect for the calculation of the total noise. If the TS-waves reach the TE, a tonal contribution is added to the overall sound in the final spectrum [1]. In this case, the dispersion of the TS-waves inside a turbulent boundary layer before reaching the TE avoids the generation of tonal noise. Hence, the study of TS-waves is a common method to determine if a laminar boundary layer transitions to turbulence.

With the aim of verifying if the domain extension was wide enough to capture all relevant flow structures, a coherence length analysis was performed. The coherence length in the source field in the spanwise direction is a key parameter in the TE noise predictions. Therefore, an evaluation of the coherence length is necessary to predict correctly the SPL radiated by the real span of the airfoil. In a statistical sense, the size of the source region which irradiates in an independent way from the closest source is represented by:

$$\gamma^2(z, \Delta z, f) = \frac{\left|\phi_{pp}(z, \Delta z, f)\right|^2}{\left|\phi_{pp}(z, 0, f)\right|\left|\phi_{pp}(z + \Delta z, 0, f)\right|} \tag{6}$$

Being z the spanwise direction and ϕ_{pp} the cross spectrum function. This function is the Fourier transform of the space-time cross correlation function:

$$\phi_{pp}(z, \Delta z, f) = \int_{-\infty}^{\infty} \langle p'(z, t) p'(z + \Delta z, t + \tau) \rangle e^{-if\tau} \, d\tau \tag{7}$$

The coherence function (γ^2) is computed from the fluctuating surface pressure p' in the vicinity of the TE. In Equation (7) the streamwise separation is fixed to obtain a function that only varies along the span with a separation Δz between consecutive points. **Figure 9** shows the spanwise pressure coherence on the suction side of the airfoil, at a location close to the TE ($x/c = 0.95$), but far enough to isolate the effects from the other side of the airfoil [14]. The spanwise distribution of the coherence function is shown for frequencies up to 10 kHz (acquisition frequency). It may be appreciated that the spanwise domain in the simulation is large enough to allow for coherence decay, as the high values of coherence are found inside a band contained well inside the simulation domain (-0.015 to 0.015). Therefore, the simulation domain may be considered a statistically independent acoustic source region.
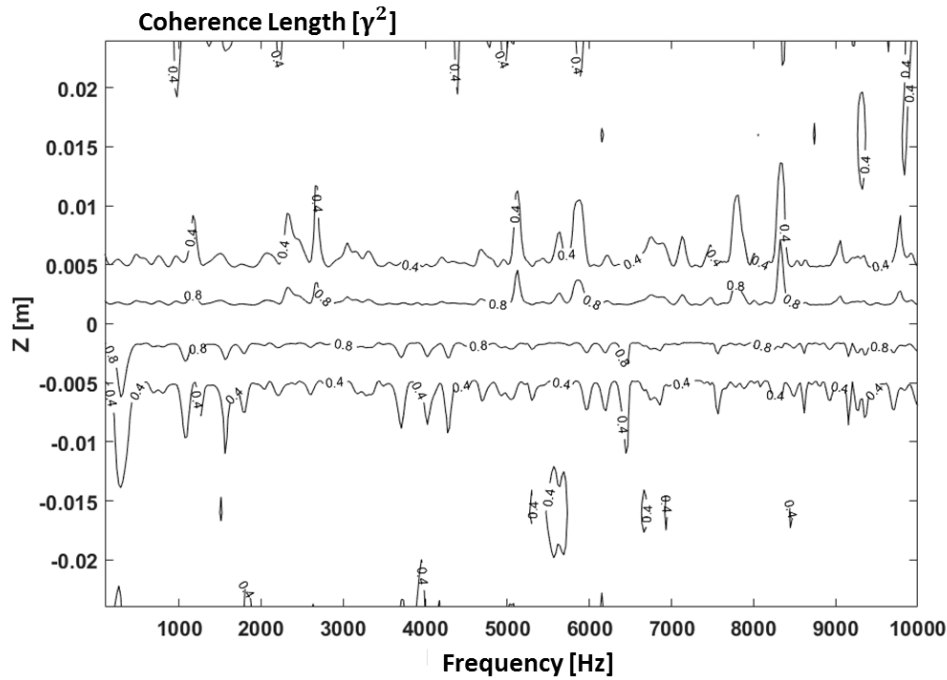
Figure 9. Iso-lines of the spanwise coherence function at x/c = 0.95 on the airfoil suction side.

6. Aeroacoustic results

After understanding the aerodynamic flow field around the airfoil and obtaining the noise source terms from the simulations every time step, Curle and FW-Hall approaches were used to predict the TE noise. Regarding Curle's analogy, the pressures over the airfoil surface are extracted from Fluent and, as well as for the FW-Hall analogy, the data are recollected every time step. The extraction period for both models corresponds to 22 through-flow times, sampling every $\Delta t = 4x10^{-5}$ s. The total N=10000 time samples are divided into 9 segments with 50 % overlap. The signals are then introduced in Equations (2) and (4) for the Curle and FW-Hall models respectively. The noise power spectra are obtained as the average of the spectra from all sampled fields. In a typical LES, the spanwise width L_z of the computational domain is only a small fraction of the actual span L_{exp}. Particularly, in this work, the simulated span is 22 times smaller than the span of the test configuration. Therefore a scaling correction based on the coherence length analysis at $x/c = 0.95$ has been applied, as suggested by Kato et al. [32]. Thus, the total SPL of the airfoil for this assumption is scaled at $(L_{exp}/L_z) \times SPL_{LES}$.

From the numerical simulations, the instantaneous pressure fluctuations on the suction and pressure sides of the airfoil are obtained. The pressure fluctuations are responsible for noise generation and are the link to aeroacoustic prediction. These fluctuations are related to the major acoustic source area near the TE, which is clearly visible in the **Figure 10**. Additionally, for the whole range of angles, these pressure fluctuations on the surface of the airfoil show a high agreement with the instability region produced when the flow transitions from laminar to turbulent regime. The vortical structures formed in the turbulent boundary layer pass by the TE and generate sound. As it may be seen, as the angle increases the pressure fluctuations on the suction side of the airfoil become higher, but on the pressure side the fluctuations are reduced. Consequently, the same behavior is expected for the SPL.
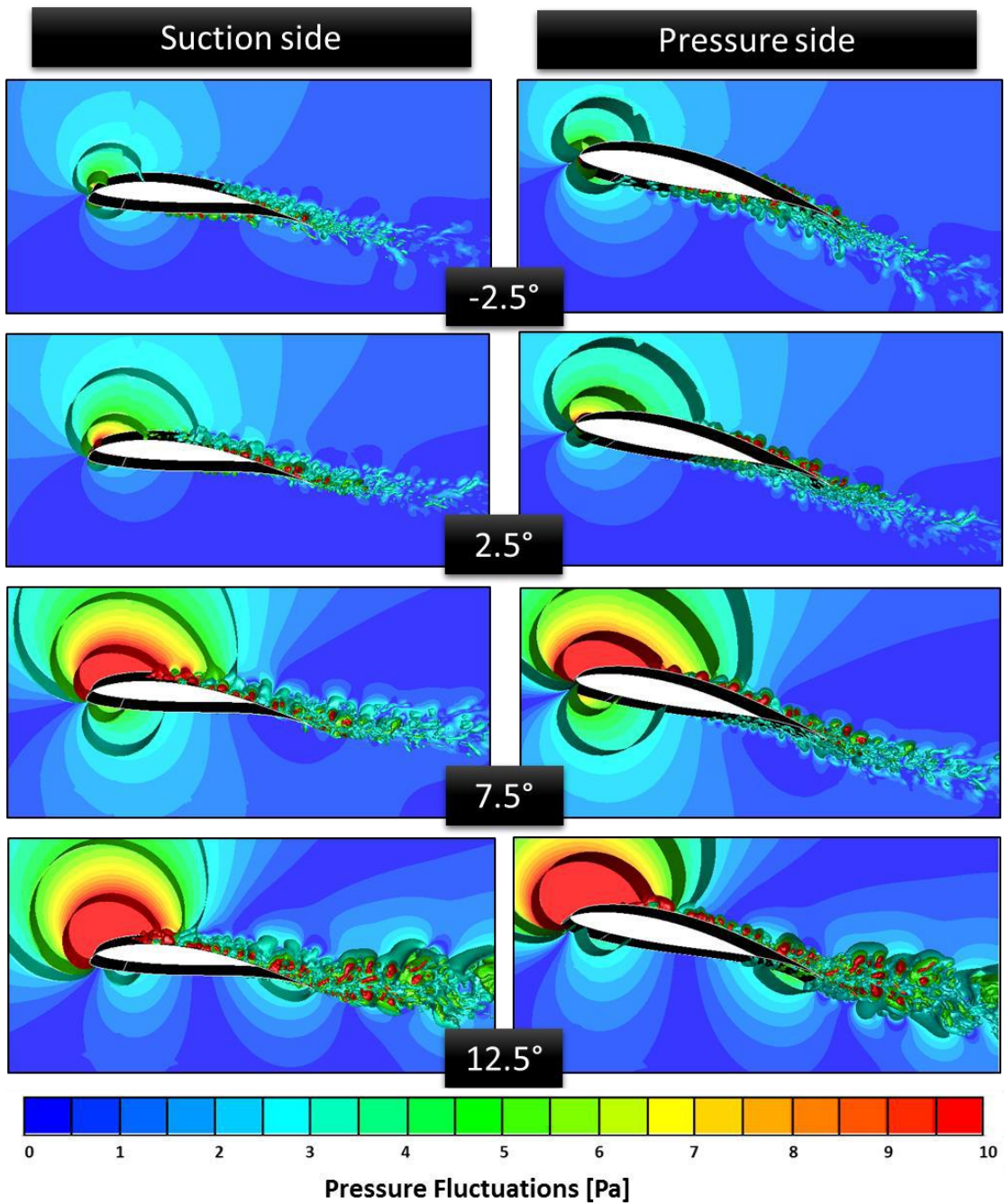
Figure 10. Numerical pressure fluctuations around the airfoil.

A crucial issue to be addressed is the aeroacoustic scattering by the airfoil TE, which is the major source of broadband noise according to experimental measurements. **Figura 11** shows the total noise (background noise + airfoil noise) against the background facility noise at the observer's position of the microphones ($R = 1.5\ m$; $\theta = 74\ deg$). The total noise is clearly above the background noise, due to the contribution of the noise produced by the airfoil to the total spectrum. Additionally, a slight increment of the total noise as the angle increases can be apreciated as well.
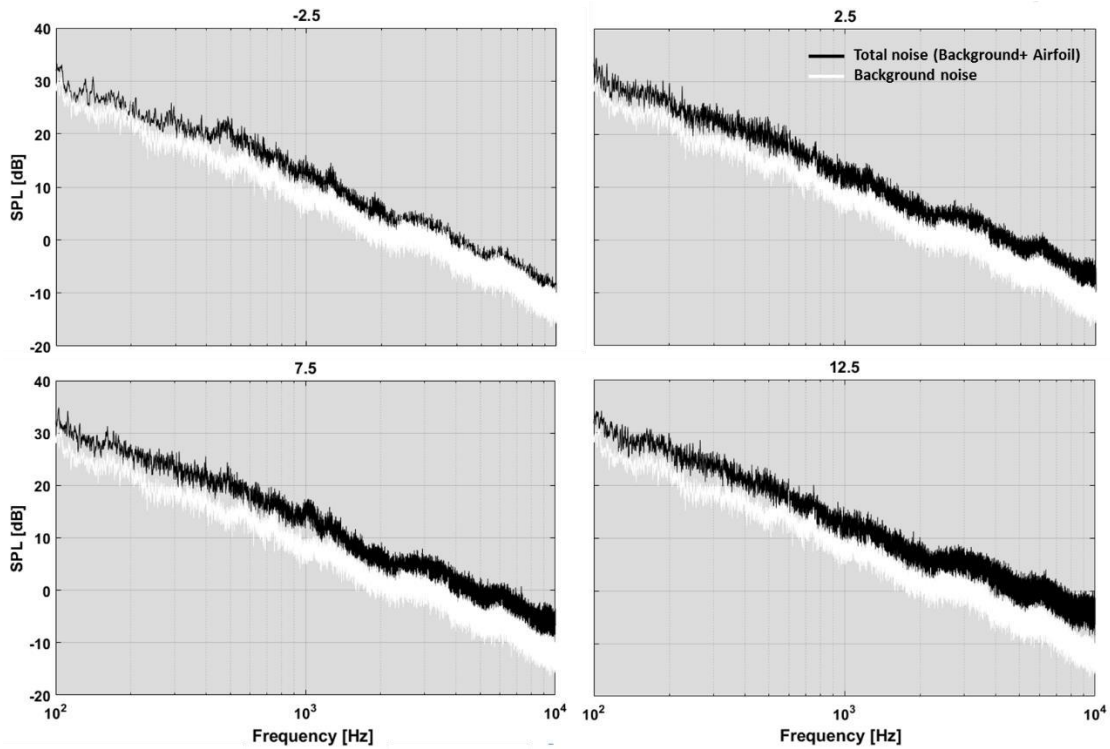
Figura 11.Comparison between total noise and background noise.

Following, the acoustic sound in the far field, computed by integration of the fluctuating physical quantities obtained from LES, is depicted in **Figure 12**. The Curle and FW-Hall models are represented in the graph, colored by blue and red respectively and compared with the TE noise extracted from the experimental measurements obtained in the aeroacoustic wind-tunnel facility. The most important feature is the abscence of tonal components in the experimental measurements. This characteristic agrees with the behavior of the boundary layer explained before, where secondary 3D instabilities are superimposed to the TS-waves and lead to a turbulent boundary layer close to the TE. Thus, the total SPL is only composed of a broadband noise contribution.

The FW-Hall model matches better the results for all the angles of attack, particulary for -2.5, 2.5 and 7.5 angles. Overall, despite the model slightly overpredicts the sound in the low and high frequencies, it follows adequately the spectrum tendency of experimental measurements, especially for $900 < f < 2500$ Hz, which correspondes with the frequency range of TE noise [4]. Regarding the data from Curle model, this model overpredicts the SPL for the whole range of frequencies. However, it follows the tendency of the experimental results up to 1 kHz, according to the results from [16]. After this frequency, a broad hump appears in the spectrum. The accuracy of Curle method depends on the precise knowledge of surface source terms, being only accurate for compact sources. Therefore, the error in the predictions may be due to the presence of a non-compact source of noise at airfoil TE. For the 12.5 degree angle, the results from the Curle model are more similar to the experimental results up to 1kHz. This effect should be further investigated in future works.

From the results, it may be deduced that the best procedure to ensure accurate acoustic predictions in the far-field for a low and intermediate angles of attack seems the FW-Hall model.
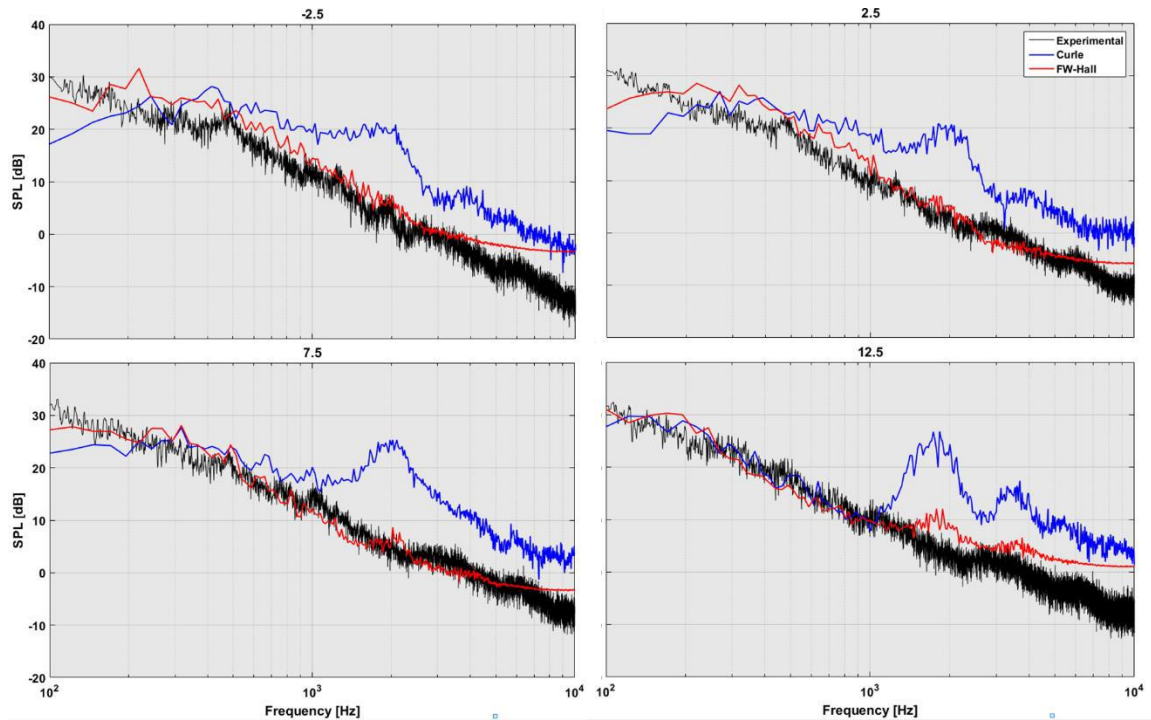
Figure 12. Comparison of the far field measurements obtained from the experiments and the Curle and FW-Hall models.

7. Conclusions

A numerical prediction of the TE noise emitted by a high-lift wind turbine airfoil (FX-63-137) for low Reynolds number for four different angles of attack has been carried out. Firstly, a CFD simulation with a wall-resolved LES modeling of the flow field for the airfoil has been completed as the initial stage of a hybrid approach. Following, pressure sources and velocity fields around the airfoil were integrated in two different acoustic models to predict the noise in the far-field region. Both aerodynamic and aeroacoustic results were validated with experimental measurements of the velocity field (via hot-wire anemometry) and the noise SPL (anechoic wind tunnel with a frequency analyzer) respectively.

An exhaustive analysis of the aerodynamic flow field has been performed in order to better understand the generation mechanisms of the TE noise. The behavior of the flow over the airfoil surface is characterized by the development of a turbulent and transient boundary layer on the suction and pressure surfaces. On both sides, the boundary layer develops 2D Tollmien-Schlichting instability waves. These waves are superimposed by secondary 3D instabilities, which lead to the development of a turbulent boundary layer close to the TE. Therefore, the turbulent flow is responsible for the TE noise production, generating a broadband spectrum.

Regarding the aeroacoustic results, the FW-Hall formulation shows a better agreement with the experiments, especially in the range of frequencies corresponding to the trailing edge, whereas Curle's analogy overpredicts airfoil sound. This overprediction may be attributed to the existence of a non-compact noise source.

The aerodynamic and aeroacoustic results presented in this work, based on the CAA, contribute to develop a more reliable and efficient acoustic prediction method. The methodology presented enables the comparison between different airfoil geometries, as well as the optimization of the shape of a given airfoil. In this way, a balance between acoustic and

aerodynamic performance may be achieved, avoiding noise problems in the vicinity of residential areas.

Acknowledgements

8. References

[1] E. Arcondoulis, C. Doolan, A. Zander y L. Brooks, «A review of trailing edge noise generated by airfoils at low to moderate Reynolds number,» *Acoustic Australia,* vol. 38, pp. 129-133, 2010.

[2] S. Oerlemans, M. Fisher, T. Maeder y K. Kögler, «Reduction of wind turbine noise using optimized airfoils and trailing-edge serrations,» *AIAA Journal,* vol. 47, nº 6, pp. 1470-1481, 2009.

[3] W. Blake, Mechanics of flow induced sound and vibration, New York: Academic Press, 1986.

[4] S. Wagner, R. Bareiss y G. Guidati, Wind turbine noise, Germany: Springer, 1996.

[5] K. Argüelles Díaz, J. Fernández Oro, E. Blanco Marigorta y C. Santolaria Morros, «Numerical prediction of tonal noise generation in an inlet vaned low-speed axial fan using a hybrid aeroacoustic approach,» *Proceedings of the Institution of Mechanical Engineers. Part C: Journal of Mechanical Engineering Science,* vol. 221, pp. 2081-2098, 2009.

[6] M. Lighthill, «On sound generated aerodynamically. Part I: General theory,» *Proceedings of the Royal Society of London,* pp. 564-587, 1952.

[7] T. Kim, M. Jeon, S. Lee y H. Shin, «Numerical simulation of flatback airfoil aerodynamic noise,» *Renewable Energy,* vol. 65, pp. 192-201, 2014.

[8] N. Curle, «The influence of solid boundaries upon aerodynamic sound,» *Procedings of the Royal Society of London,* vol. 231, pp. 505-514, 1955.

[9] R. Amiet, «Noise due to turbulent flow pas a trailing edge,» *Journal of Sound and Vibration,* vol. 47, nº 3, pp. 387-393, 1976.

[10] J. Ffowcs Williams y L. Hall, «Aerodynamic sound generation by turbulent flow in the vicinity of a scattering half plane,» *Journal of Fluid Mechanics,* vol. 40, pp. 657-670, 1970.

[11] M. Howe, «Trailing edge noise at low mach numbers,» *Journal of Sound and Vibration,* vol. 225, nº 2, pp. 211-238, 1999.

[12] M. Wang, «Computation of trailing edge noise at low mach number using LES and acoustic analogy,» *Center for turbulence research. Annual Research Briefs,* 1998.

[13] J. Christophe, J. Anthonie y S. Moreau, «Trailing edge noise of a controlled diffusion airfoil at moderate and high angle of attack,» de *15th AIAA/CEAS Aeroacoustics Conference*, Miami,FL, 2009.

[14] J. Winkler, S. Moreau y T. Carolus, «Airfoil trailing edge noise prediction from Large Eddy Simulation: Influence of grid resolution and noise model formulations,» de *16th AIAA/CEAS Aeroacoustics Conference*, Stockholm, 2010.

[15] H. Kim, S. Lee y N. Fujisawa, «Computation of unsteady flow and aerodynamic noise of NACA0018 airfoil using large-eddy simulation,» *International Journal of Heat and Fluid Flow,* vol. 27, pp. 229-242, 2006.

[16] J. Winkler, S. Moreau y T. Carolus, «Large eddy simulation and trailing edge noise prediction of an airfoil with boundary layer tripping,» de *15th AIAA/CEAS Aeroacoustics Conference*, Miami,FL, 2009.

[17] M. Howe, «Noise produced by a sawtooth trailing edge,» *Journal of the Acoustical Society of America,* vol. 1, nº 1, pp. 482-487, 1991.

[18] M. Herr, «Design criteria for low-noise trailing edges,» de *28th AIAA Aeroacoustics Conference, Paper 2007-3470.*, 2007.

[19] T. Lutz, A. Herrig, W. Würz, M. Kamruzzaman y E. Krämer, «Design and wind tunnel verification of low airfoils for wind turbines,» *AIAA Journal,* vol. 45, nº 4, pp. 779-792, 2007.

[20] D. Althaus y F. Wortmann, «Stuttgarter Profilkatalog,» Institut für Aerodynamik, German, 1972.

[21] M. Lastra, J. Fernández Oro, M. Galdo Vega, E. Blanco Marigorta y C. Santolaria Morros, «Novel design and experimental validation of a contraction nozzle for aerodynamic measurements in a subsonic wind tunnel,» *Journal of Wind Engineering and Industrial Aerodynamics,* vol. 118, pp. 35-43, 2013.

[22] C. Bailly y G. Comte-Bellot, Experimental Fluid Mechanics, Springer, 2015.

[23] E. Blanco, R. Ballesteros y C. Santolaria, «Angular range and uncertainty analysis of non-orthogonal crossed hot wire probes,» *Journal of Fluids Engineering,* vol. 120, pp. 90-94, 1998.

[24] J. Fernández Oro, K. Díaz Argüelles, C. Santolaria Morros y E. Blanco Marigorta, «Unsteady flow and wake transport in a low speed axial fan with inlet guide vanes,» *Journal of Fluids Engineering,* vol. 129, pp. 1015-1029, 2007a.

[25] C. Allen, W. Blake, R. Dougherty, D. Lynch, P. Soderman y J. Underbrink, Aeroacoustic measurements, Berlin: Springer, 2002.

[26] S. Moreau, M. Henner, G. Iaccarino, M. Wang y M. Roger, «Analysis of Flow Conditions in Freejet Experiments,» *American Institute of Aeronautics and Astronautics Journal,* vol. 41, nº 10, pp. 1895-1905, 2003.

[27] C. Wagner, T. Hullt y P. Sagaut, Large eddy simulation for Acoustics, UK: Cambridge University Press, 2007.

[28] S. Dahlstrom y L. Davidson, «Large eddy simulation of the flow around an Aerospatiale aerofoil,» de *European Congress on Computational Methods in Applied Sciences and Engineering,11-14 September*, Barcelona, 2000.

[29] M. Wang y P. Moin, «Computation of trailing-edge flow and noise using large-eddy simulation,» *AIAA Journal,* vol. 38, nº 12, pp. 2201-2209, 2000.

[30] K. Argüelles Díaz, I. Solís-Gallego, A. Meana Fernández, J. Fernández Oro y S. Velarde-Suárez, «Turbulence structure around an asymmetric high-lift airfoil for different incidence angles (acepted for publication),» *Journal of Applied Fluid Mechanics,* vol. 10, nº 4, 2017.

[31] J. Winkler, T. Carolus y S. Moreau, «Airfoil trailing edge blowing: Broadband noise prediction from large eddy simulation,» de *In Proceedings of the 15th AIAA/CEAS Aeroacoustics Conference*, 2009.

[32] C. Kato, A. Iida, Y. Takano, H. Fujita y M. Ikegawa, «Numerical prediction of aerodynamic noise radiated from low Mach number turbulent wake,» *AIAA Journal,* pp. 93-0145, 1993.